frontiers | Frontiers in Physics

TYPE Original Research
PUBLISHED 11 May 2023
DOI 10.3389/fphy.2023.1153645

OPEN ACCESS

EDITED BY
Kh S. Mekheimer,
Al-Azhar University, Egypt

REVIEWED BY
Ebenezer Bonyah,
University of Education, Winneba, Ghana
Ali Mohammed Moawad,
Al-Azhar University, Egypt

*CORRESPONDENCE
Sardar Bilal,
sardarbilal@mail.au.edu.pk

SPECIALTY SECTION
This article was submitted to Statistical and Computational Physics, a section of the journal Frontiers in Physics

RECEIVED 29 January 2023
ACCEPTED 27 March 2023
PUBLISHED 11 May 2023

CITATION
Bilal S, Khan NZ and Eldin SM (2023), FEM analysis of the impact of surface undulations on the natural convective flow of viscous fluid in a permeable trapezoidal enclosure.
Front. Phys. 11:1153645.
doi: 10.3389/fphy.2023.1153645

RETRACTED: FEM analysis of the impact of surface undulations on the natural convective flow of viscous fluid in a permeable trapezoidal enclosure

Sardar Bilal[1]*, Noor Zeb Khan[1] and Sayed M. Eldin[2]

[1]Department of Mathematics, Air University, Islamabad, Pakistan, [2]Center of Research, Faculty of Engineering, Future University in Egypt, New Cairo, Egypt

Examination of the transport mechanism in a permeable trapezoidal enclosure with an undulation effect is commenced. A formulation describing naturally convective flow in a permeable domain is conceded by employing Boussinesq and Darcy approximations. Uniform temperature is provided at the circular cylinder and base wall of the enclosure, whereas non-parallel side extremities are kept cold. No heat flux condition is applied at a wavy surface (upper) to maintain the potential difference in temperature for generation of convection. A finite element scheme is opted to resolve the governing system for accounted physical problems. The grid sensitivity test is also executed to assure the credibility of the code and results. A wide range of physical parameters is selected to comprehend their impact on streamlines and isotherm patterns. Results are revealed comparatively for zero undulation (upper solid straight wall) and with undulations (wavy wall). Heat flux and kinetic energy are also enumerated as key quantities against concerning parameters. It is depicted that the average Nusselt number and kinetic energy are more in the absence of undulations than when it is present. Additionally, it is manifested that the placement of a heated cylinder helps transfer heat in the domain and the production of thermal convective potential.

KEYWORDS

permeability aspects, natural convection., undulations, circular cylinder, FEM

1 Introduction

Realistic monitoring of dynamics of liquid flow is in permeable medium instead of consideration of the solid domain. Abundant procedures, such as contaminant removal, building insulation, geothermal systems, filtration procedures, removal of wastes in nuclear plants and reactors, and biofilm growth, are common examples of material flow in permeable media. Henry Darcy laid the basis for transport evaluation in the porous domain by characterizing a law that delineates the flow description of water by accounting low magnitude of inertial forces. Continuing the work of Darcy, Beavers and Joseph [1] developed a constraint at the interface of fluid and homogenous medium interaction. Pulikatos [2] documented convective thermal transport in the permeable medium by analyzing the impact of the Rayleigh number on flow and thermal attributes. An experimental study to assess the performance of naturally convective fluid flow in an enclosure partially filled with a vertical layer of the saturated permeable medium was

conducted by Beckermann et al. [3, 4]. The onset of convection in porous layers by considering the critical range of Rayleigh numbers was inferred by Chen and Chen [5]. Coupling of the thermofluid characteristics of viscous fluid in a permeable medium with differentially heated walls was adumbrated by Breton [6]. Singh and Thorpe [7] compared two different models (the Darcy and extended Darcy models) for free convection in the fluid by applying Beavers–Joseph conditions at the interface. Webster et al. [8] described the sedimental transport of material through pores and the convection to measure salinity around the permeable surface. Goyeau et al. [9] discussed momentum balance for the transition layer formed at the interface of liquid and porous substrate and measured the stress jump coefficient. Goyeau et al. [9] conducted momentum transfer at the interface of permeable and homogeneous domains by employing the jump condition and developing a volume-averaged equation. Gobin et al. [10] depicted opposing/assisting flow in an enclosure saturated with a vertical porous layer. Shah and Asad [11] analyzed the influence of forced convection on hydrothermal attributes of ferrofluid enclosed in the permeable enclosure by utilizing the Darcy law. Lund et al. demonstrated the magnetically influenced nanofluid flow over a permeable exponential surface by incorporating the modified Darcy expression [12]. Inspection of dynamics of thermally stratified viscous fluid under multiple physical aspects (variable viscosity, thermal conductivity, and MHD) over a permeable paraboloid surface with entropy generation was manifested by Rooman et al. [13]. Studies on flow and thermal attributes in permeable media are disclosed in [14–20].

Transmission of heat in permeable media develops the coupling of thermomechanical problems, which occurs in multiple scientific problems. Some examples are in building insulation, performance of mechanical devices (washing machines, heat exchangers, and fuses); performance of biomedical instruments; and large-scale procedures (nuclear reactors and power plants). In addition, the influential role of convective transport in porous domains is also addressed in geological systems for controlling the flow of volcanic lavas and extraction of minerals from rocks [21, 22]. Use of convection in permeable environments in the production of geothermal energy was disused in [23]. After examining the physical significance of convective heat transfer in permeable configurations, an extensive deal of work has been manifested. Similarly, Molla et al. [24] scrutinized the flow characteristics of the fluid filled in the porous enclosure with the impact of localized heating using the finite volume approach. Enhancement in convective heat transfer with the induction of copper nanoparticles in the permeable enclosure was explicated by Alhashah and Saleh [25]. Enhancement in the heat transfer rate of non-Newtonian fluid flow over a stretching sheet with the induction of nanoparticles was probed by Abdullah et al. [26]. Sensitivity analysis by executing a computational approach to investigate magnetized nanofluid flow over an exponentially stretchable surface was explored by Shahid et al. [27]. Some recently published work in accordance with the convective mechanism in porous enclosures [28–30] is enclosed for the interest of readers.

An intensive overview of available work acknowledges that the study of convective transport in the permeable medium is restricted to enclosures with straight boundaries. However, flow and thermal analyses in permeable enclosures with wavy extremities are scantly considered. Keeping in mind the vast usage of permeable enclosures with wavy boundaries in thermal engineering procedures, the authors become inspired wholeheartedly to scrutinize free convective energy transportation inside the trapezoidal enclosure by considering permeability aspects along with variation in the aspect ratio of a heated circular cylinder. Results are revealed in the form of streamlines and isothermal contour plots against the Darcy parameter (Da), Rayleigh number (Ra), and Prandtl number (Pr). The local and average heat flux coefficient at the lower wall is also computed. The originalities of the present work are as follows:

- The geometry recognizes complex permeable medium enclosure (trapezoidal-shaped enclosure with upper wavy wall and emplaced by a hot circular cylinder).
- Impact of undulations on flow characteristics will be encapsulated.
- Thermodynamical coupling of fluid flow in the chamber will be discussed in a permeable environment.

According to the authors' knowledge, this is a worthy research effort and will help investigators.

2 Mathematical model

2.1 Problem description

Here, the 2D steady, incompressible, and laminar flow of viscous fluid in the trapezoidal enclosure is assumed. The Darcy law is employed to envisage permeability aspects by obliging low Reynold number assumption to minimize the impact of inertial forces. Undulations are considered at the upper wall of the enclosure. Boussinesq approximation is used to interpret the convection phenomenon in the domain and consider the density to be impersistent. Graphical visualization of the considered problem is displayed in Figure 1.

2.2 Governing equations

Constitutive equations after employing all assumptions are as follows [31]:

$$u_X + v_Y = 0, \tag{1}$$

$$uu_X + vu_Y = -\frac{1}{\rho}p_X + \upsilon[u_{XX} + u_{YY}] - \frac{\upsilon}{\kappa}u, \tag{2}$$

$$uv_X + vv_Y = -\frac{1}{\rho}p_Y + \upsilon[v_{XX} + v_{YY}] + g\beta(T - T_c) - \frac{\upsilon}{\kappa}v, \tag{3}$$

$$uT_X + vT_Y = \alpha[T_{XX} + T_{YY}]. \tag{4}$$

Associated boundary constraints are as follows:

$$\begin{aligned} &u(X,Y) = 0 = v(X,Y), 0 \le X \le L, 0 \le Y \le L \\ &\text{On the top horizontal wall} \quad \frac{\partial T}{\partial y}(X,Y) = 0, \\ &\text{On the bottom horizontal wall} \quad T(X,Y) = T_h, \\ &\text{On the left \& right vertical walls} \quad T(X,Y) = T_c. \end{aligned} \tag{5}$$

The subsequent dimensionless variables related to the Newtonian natural convection fluid model in the permeable medium are introduced:

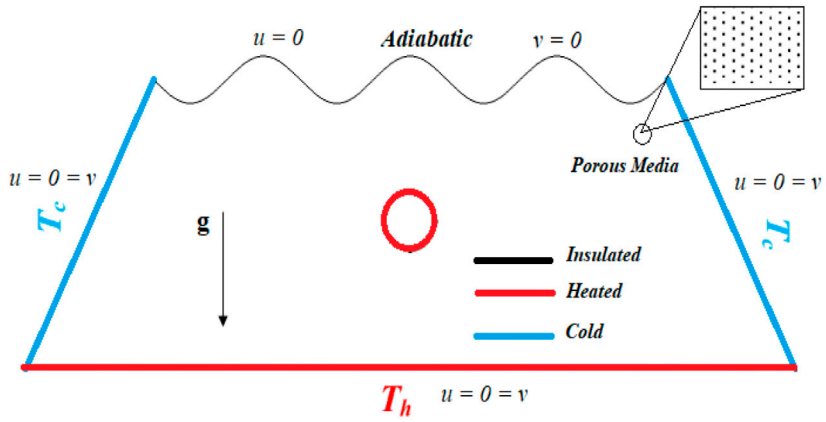

FIGURE 1
Display of enclosure with boundary constraint.

$$\breve{X} = \frac{X}{L}, \breve{Y} = \frac{Y}{L}, \breve{U} = \frac{uL}{\alpha}, \breve{V} = \frac{vL}{\alpha}, \breve{P} = \frac{pL^2}{\rho\alpha^2}, \breve{\theta} = \frac{T - T_c}{\Delta T} \quad (6)$$

The dimensional forms of governing equations are as follows:

$$\breve{U}_{\breve{X}} + \breve{V}_{\breve{Y}} = 0, \quad (7)$$

$$\breve{U}\breve{U}_{\breve{X}} + \breve{V}\breve{U}_{\breve{Y}} = -\breve{P}_{\breve{X}} + \Pr\left[\breve{U}_{\breve{X}\breve{X}} + \breve{U}_{\breve{Y}\breve{Y}}\right] - \frac{\Pr}{P}\breve{U}, \quad (8)$$

$$\breve{U}\breve{V}_{\breve{X}} + \breve{V}\breve{V}_{\breve{Y}} = -\breve{P}_{\breve{Y}} + \Pr\left[\breve{V}_{\breve{X}\breve{X}} + \breve{V}_{\breve{Y}\breve{Y}}\right] + Ra\Pr - \frac{\Pr}{P}\breve{V}, \quad (9)$$

$$\breve{U}\breve{\theta}_{\breve{X}} + \breve{V}\breve{\theta}_{\breve{Y}} = \breve{\theta}_{\breve{X}\breve{X}} + \breve{\theta}_{\breve{Y}\breve{Y}} \quad (10)$$

On each of the four walls forming the boundaries $\breve{U}(\breve{X}, \breve{Y}) = 0 = \breve{V}(\breve{X}, \breve{Y})$, $0 \le \breve{X} \le 1$, $0 \le \breve{Y} \le 0.55$,

$$\begin{aligned} &\text{On the top horizontal wall} \quad \breve{\theta}_{\breve{Y}}\left(\breve{X}, \breve{Y}\right) = 0, \\ &\text{On the bottom horizontal wall} \quad \breve{\theta}\left(\breve{X}, \breve{Y}\right) = 1, \\ &\text{On left and right vertical walls} \quad \breve{\theta}\left(\breve{X}, \breve{Y}\right) = 0. \end{aligned} \quad (11)$$

Involved physical parameters are mentioned as follows:

$$\begin{aligned} &\text{Prandtl number } \Pr = \frac{\upsilon}{\alpha}, \\ &\text{Rayleigh number } Ra = \frac{g\beta\Delta TL^3}{\alpha\upsilon}, \\ &\text{Darcy number } P = \frac{\kappa}{L^2}. \end{aligned} \quad (12)$$

2.3 Quantities of interest

The rate of heat transfer is expressed in terms of the local Nusselt number (Nu_{Local}) as follows:

$$Nu_{Local} = \left(-\frac{\partial\breve{\theta}}{\partial\breve{X}}\right)_{\breve{X}=0} \quad (13)$$

The average Nusselt number (Nu_{Avg}), which is a global physical quantity, is addressed as follows:

$$Nu_{Avg} = \frac{1}{S}\int_S Nu_{Local}dS \quad (14)$$

Total kinetic energy is mathematically expressed as follows:

$$K.E = \frac{1}{2}\int_\Omega \|u\|^2 d\Omega \quad (15)$$

3 Computational scheme

In this segment, the basic components related to the implemented numerical scheme (finite element method) are described. Compared to the finite difference method currently used, the numerical scheme is more efficient in simulating results because the traditional method (FDM) works on simpler problems. The finite element method is more advantageous because it is applied to a complex structure domain and will compute associated physical quantities even singularity exists, either in the domain or on the boundaries. To implement the finite element method, the discretization of the domain is first performed. For this purpose, the 2D domain is discretized into triangular and rectangular elements, and grid sensitivity text is executed to form the credibility of the work (see Figure 2). The rest of all computations are evaluated at refinement levels where the physical quantity shows consistent results. Afterward, the developed model is solved at each element level, and a local stiffness matrix is formed. Later, these equations are combined to create a global stiffness matrix, and finally, a system of non-linear equations is generated. These formulated equations are tackled using the Newton–Raphson method. The described method is step-wise presented in Figure 3.

The following convergence criterion is set for the non-linear iterations:

$$\left|\frac{\chi^{n+1} - \chi^n}{\chi^{n+1}}\right| < 10^{-6},$$

where χ designates the universal solution component.

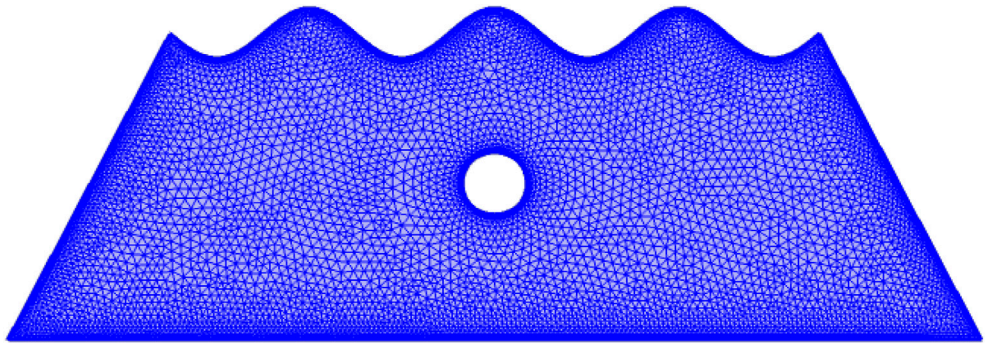

FIGURE 2
Extra-fine grid for a wavy trapezoidal cavity with the heated cylinder.

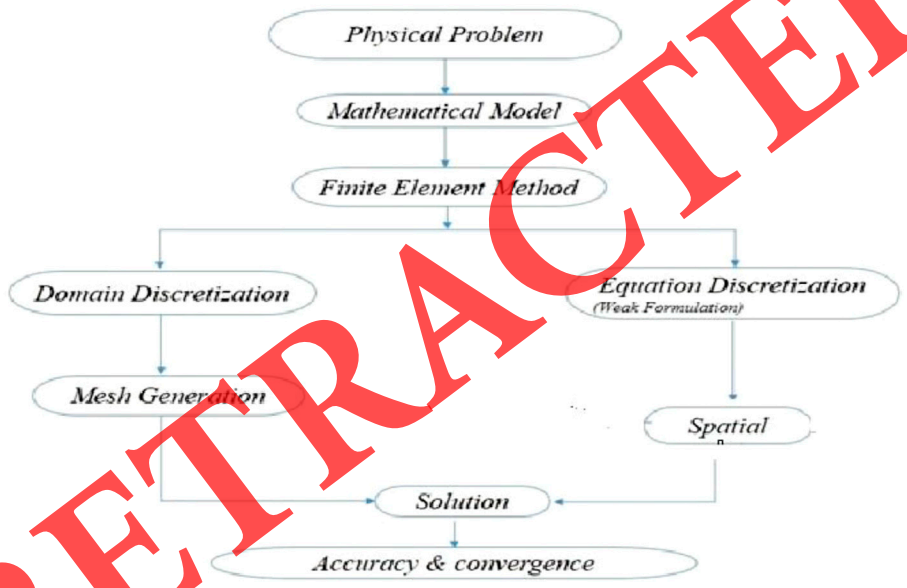

FIGURE 3
Schematic diagram of the finite element method.

Table 1 deliberated the number of elements (#E) and degree of freedom (DOF) against the different refinement levels. It is noted that both (#E) and (DOF) are increases for different refinement levels

3.1 Grid convergence

A grid convergence test is performed at various grid levels by restricting $Pr = 0.71, P = 10^{-3}, and\ Ra = 10^3$ to show the efficiency of the obtained results, as shown in Table 2. For this purpose, the average Nusselt number (Nu_{Avg}) is computed. At levels 8 and 9, the values of the mentioned quantities of engineering interest show agreement with each other.

4 Result and discussion

An investigation on the impact of the Rayleigh number (***Ra***), Prandtl number (***Pr***), Darcy number (***P***), and the number of undulations ($\boldsymbol{\lambda}$) of the permeable wavy trapezoidal enclosure was conducted. The steady-state versions of the streamlines, temperature distributions, and local heat flux were presented to evaluate these field variables. The following dimensionless group parametric domains were considered in the current numerical investigation: $(10^{-3} \le P \le 10^{-5})$, $(10^3 \le Ra \le 10^5)$, $(0.015 \le Pr \le 7.000)$, and $(0 \le \lambda \le 4)$. Figures 4–12 demonstrate isotherms, streamlines, local Nusselt numbers, and average Nusselt numbers for various values of the governing parameters indicated previously. The effects of the number of undulations (λ) from the top to bottom and Prandtl

TABLE 1 Number of elements and degree of freedom at different refinement levels.

R. Levels	$\lambda = 0$		$\lambda = 1$		$\lambda = 2$		$\lambda = 3$		$\lambda = 4$	
	# E	DOF	# E	DOF	# E	DOF	# E	DOF	# E	DOF
R_1	38,127	207,374	37,422	203,863	34,199	186,586	34,397	187,800	34,775	189,998
R_2	14,949	83,420	14,606	81,719	13,228	74,213	13,355	74,974	13,360	75,153
R_3	6,143	34,798	6,074	34,467	5,424	30,965	5,394	30,871	5,625	32,124
R_4	3,732	21,945	3,587	21,234	3,325	19,728	3,356	19,925	3,522	20,839
R_5	2,550	15,391	2,504	15,161	2,323	14,102	2,319	14,110	2,538	15,359
R_6	1,385	8,712	1,357	8,572	1,252	7,949	1,304	8,237	1,451	9,126
R_7	884	5,801	870	5,731	816	5,377	823	5,426	937	6080
R_8	522	3,543	488	3,373	465	3,188	482	3,287	544	3681
R_9	296	2,077	292	2,057	276	1,949	314	2,167	369	2540

Bold values means that the variation are measured against that parameters specially.

TABLE 2 Grid convergence study for the mean Nusselt for $P = 0.001$, $Pr = 0.710$, and $Ra = 10^3$.

Refinement level	Nu_{Avg}
L_1	5.0279
L_2	5.9687
L_3	6.7624
L_4	7.2440
L_5	7.9412
L_6	8.4068
L_7	10.8608
L_8	11.4650
L_9	11.4650

Bold values means that the variation are measured against that parameters specially.

numbers (Pr) from left to right on the momentum and energy transport mechanism in the permeable enclosure are explored by plotting isotherm contours, as shown in Figure 4 at $Ra = 10^3$ and $P = 10^{-3}$. The increase in Pr from 0.015 to 7.000 will cause dominancy in momentum diffusivity due to the kinetic energy that causes increase in heat transfer. At lower magnitude of $Pr = 0.015$, the isotherm concentration is detached from the boundaries and lies in the top portion of the enclosure, but a contrary aspect is seen at a higher magnitude of $Pr = 7.00$. Furthermore, the number of undulations has an inverse relation with heat transfer, as by varying λ from 0 to 4, the top adiabatic wall will change from a flat to a wavy surface, which decreases heat transfer. $\lambda = 0$ has a flat top adiabatic wall, which is far away from the heated circular cylinder. The increase in λ will change the flat surface into a crest and trough, where the trough comes closer to the heated surface and limits heat flux.

Figure 5 illustrates the velocity field for the effects of the number of undulations (λ) from the top to bottom and Prandtl numbers (Pr) from left to right at $Ra = 10^3$ and $P = 10^{-3}$. A couple of circulation eddies appear inside the enclosure. In the right half side of the cavity, the streamlines raise up with the heated cylinder and fall along the vertical cold wall, forming a roll within the cavity rotated clockwise. A similar roll is formed with anti-clockwise rotations on the left half side of the cavity. With a increase in the Prandtl number (Pr) from 0.015 to 7.000, the circulation cell decreases the middle rotation's flow pattern, which changes into an oval shape and covers up the whole cavity. Subsequently, five different magnitudes of the number of undulations are entertained by varying from $0 \le \lambda \le 4$. However, the remaining parameters are kept constant by specifying the value of $Ra = 10^3$ and $P = 10^{-3}$. Streamlines have an inverse relation with the number of undulations, as varying λ from 0 to 4, the top adiabatic wall will change from a flat to a wavy surface. Two circular-shaped eddies are created for $\lambda = 0$ flattop adiabatic wall. The increase in λ from 1 to 4 will change the flat into a wavy, crest and trough surface, and the eddies entered the crest, which causes decreases in the middle rotation's flow pattern and change the shape of eddies from circular to oval.

The joint influence in temperature field against the Darcy number (P) and the number of undulations (λ) from left to right and top to bottom, respectively, on the momentum and energy transport mechanism in the permeable enclosure is explored by plotting isotherm contours, as shown in Figure 7 at $Ra = 10^3$ and $Pr = 0.710$. As P is the ratio of permeability (κ) to square of characteristic length (L^2), P has a direct relation with permeability (κ); the increase in P will increase the number of pores in the medium, which causes an increment in the momentum diffusivity and kinetic energy. As a result, the magnitude of temperature is increased. Permeability is used to enhance the flow rate. The decrease in P from 10^{-3} to 10^{-5} will reduce from an irregular shape, which covers the encompassing a smooth curve at the middle of the cavity. Furthermore, the temperature has an inverse relation with the number of undulations; the increase in λ from 0 to 4 will change the upper horizontal wall from a flat to a wavy surface, which causes a decrease in heat transfer. $\lambda = 0$ has a flat top adiabatic wall far away from the heated circular cylinder whereby heat will

10.3389/fphy.2023.1153645

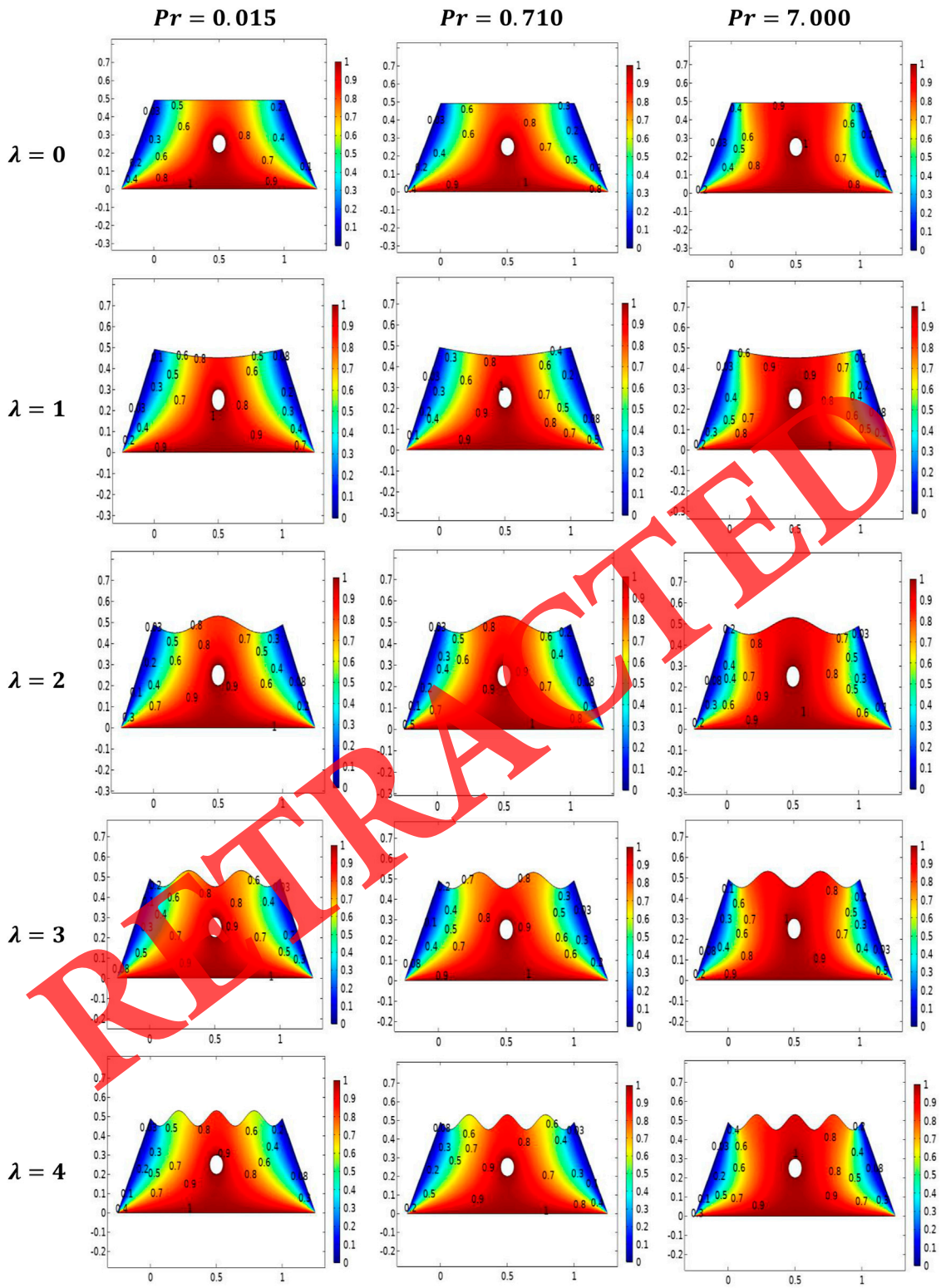

FIGURE 4
Isotherm variation for the number of undulations against the Prandtl number (*Pr*).

flow freely. However, the increase in λ from 1 to 3 will change the flat surface to a wavy one, that is, crest and trough surface, where the trough closer to the heated surface causes blockage of heat transfer.

The mixed variations in the velocity field against the number of undulations (λ) and the Darcy number (P) in view of the streamline field are shown in Figure 7. The streamlines rise from the heated bottom with the heated cylinder on the right and lift sides of the

10.3389/fphy.2023.1153645

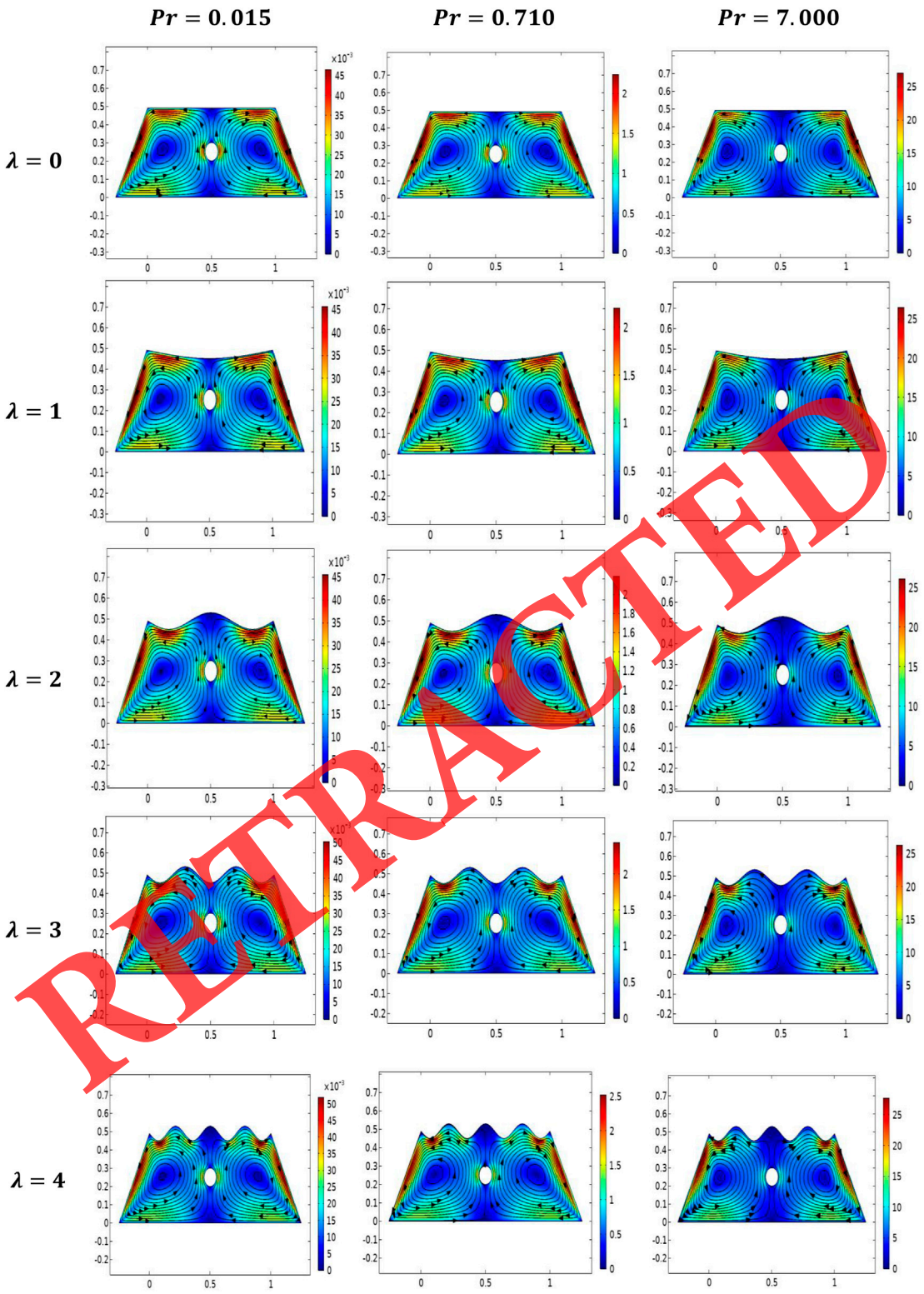

FIGURE 5
Streamline variation for the number of undulations against the Prandtl number (*Pr*).

cavity and descend along the vertical cold wall, generating two rolls inside the cavity that are spun in opposite directions. Furthermore, the rolls become elliptic and cover up the whole cavity for the highest magnitude of the Darcy number (P). With a decrease in the Darcy number (P) from 10^{-3} to 10^{-5}, permeability decreases by a factor of 10^{-1} and the flow rolls decrease the middle rotation's flow pattern,

10.3389/fphy.2023.1153645

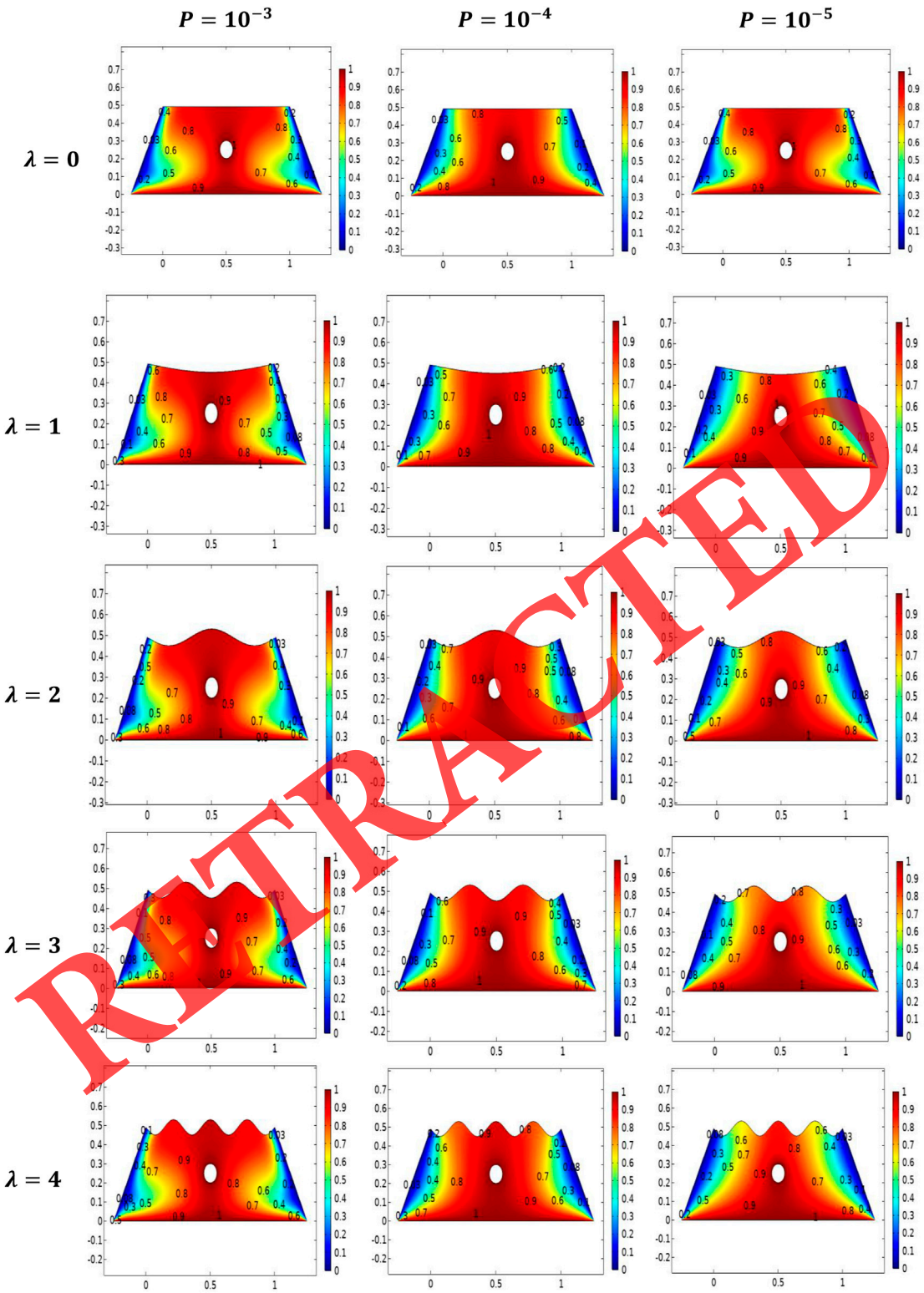

FIGURE 6
Isotherm variation for the number of undulations (λ) against the Darcy number (P).

which changes into an oval contour and covers up the whole cavity. Eventually, in the range of $0 \leq \lambda \leq 4$, five distinct numbers of undulations are entertained. However, the remaining parameters are kept constant by specifying the value of $Ra = 10^3$ and $P = 10^{-3}$. It is evident that the number of undulations has an inverse relationship with streamlines; a horizontal top adiabatic wall will

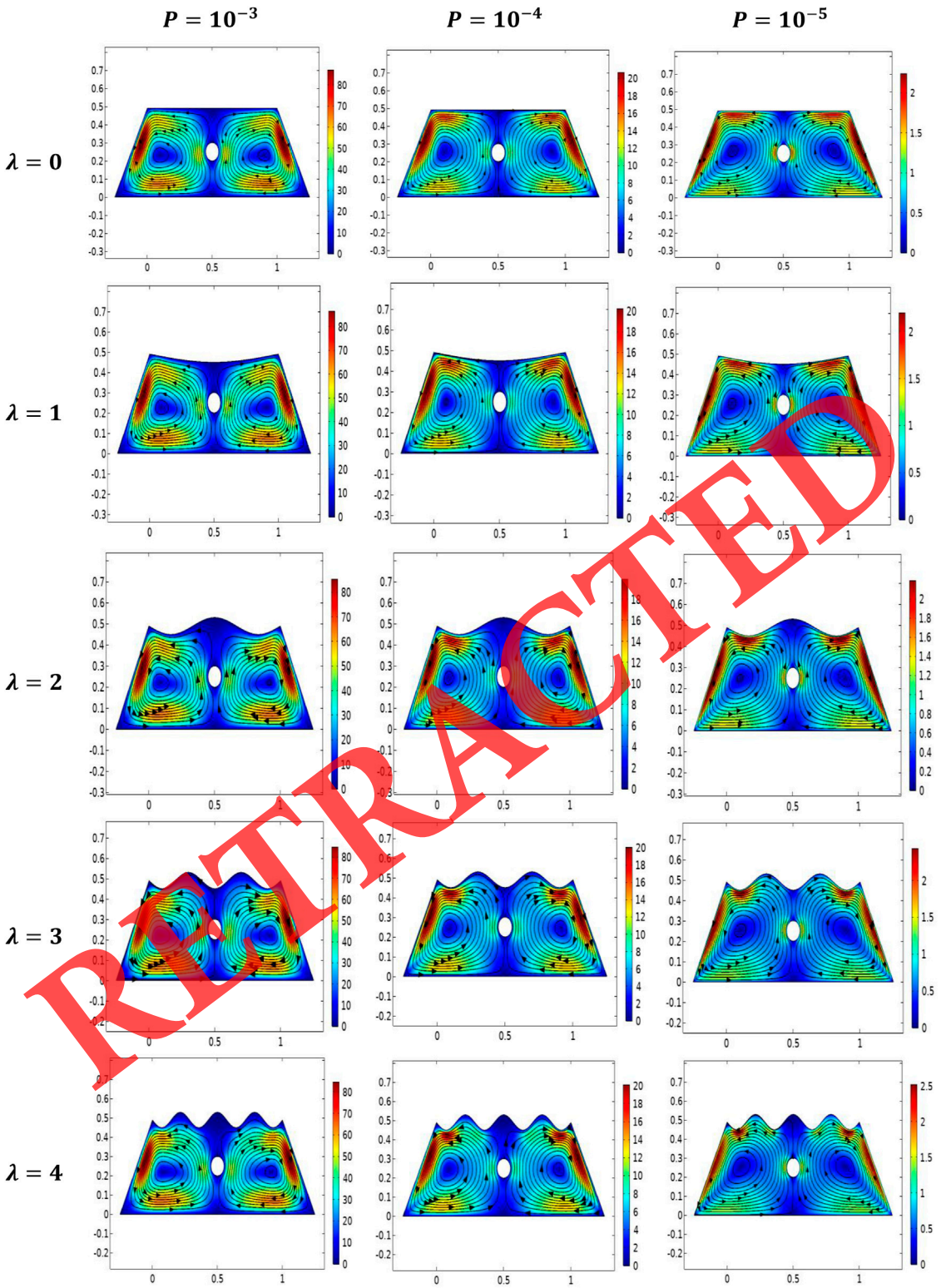

FIGURE 7
Streamline variation for the number of undulations against the Darcy number (P).

change from a flat to a wavy surface by changing (λ) from 0 to 4. Two circular-shaped eddies are generated with the flat top of the adiabatic wall for $\lambda = 0$. The increase in λ, from 1 to 4, will change the flat into a wavy, that is, crest and trough surface and eddies entered the crest, which decreases the middle rotation's flow pattern and changes the shape of eddies from circular to oval.

10.3389/fphy.2023.1153645

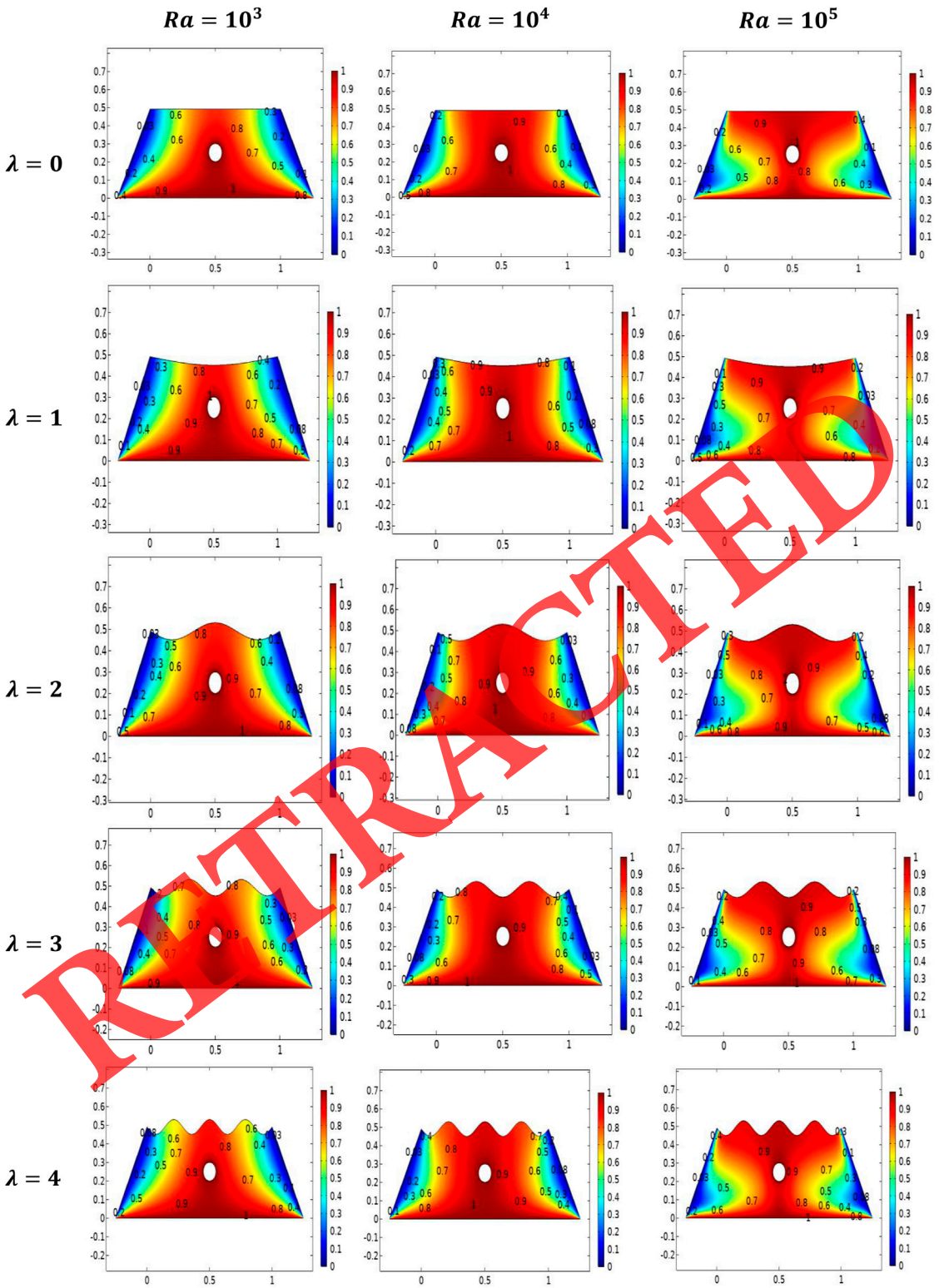

FIGURE 8
Isotherm variation for the number of undulations against the Rayleigh number (*Ra*).

The paired influence in the temperature field against the Rayleigh number (*Ra*) from left to right and the number of undulations (λ) from top to bottom in sight of the isotherm contour is displayed in Figure 8. From left to right, $10^3 \leq Ra \leq 10^5$ increases, and the convection heat transfer takes over as the predominant mode inside the cavity, causing extra

10.3389/fphy.2023.1153645

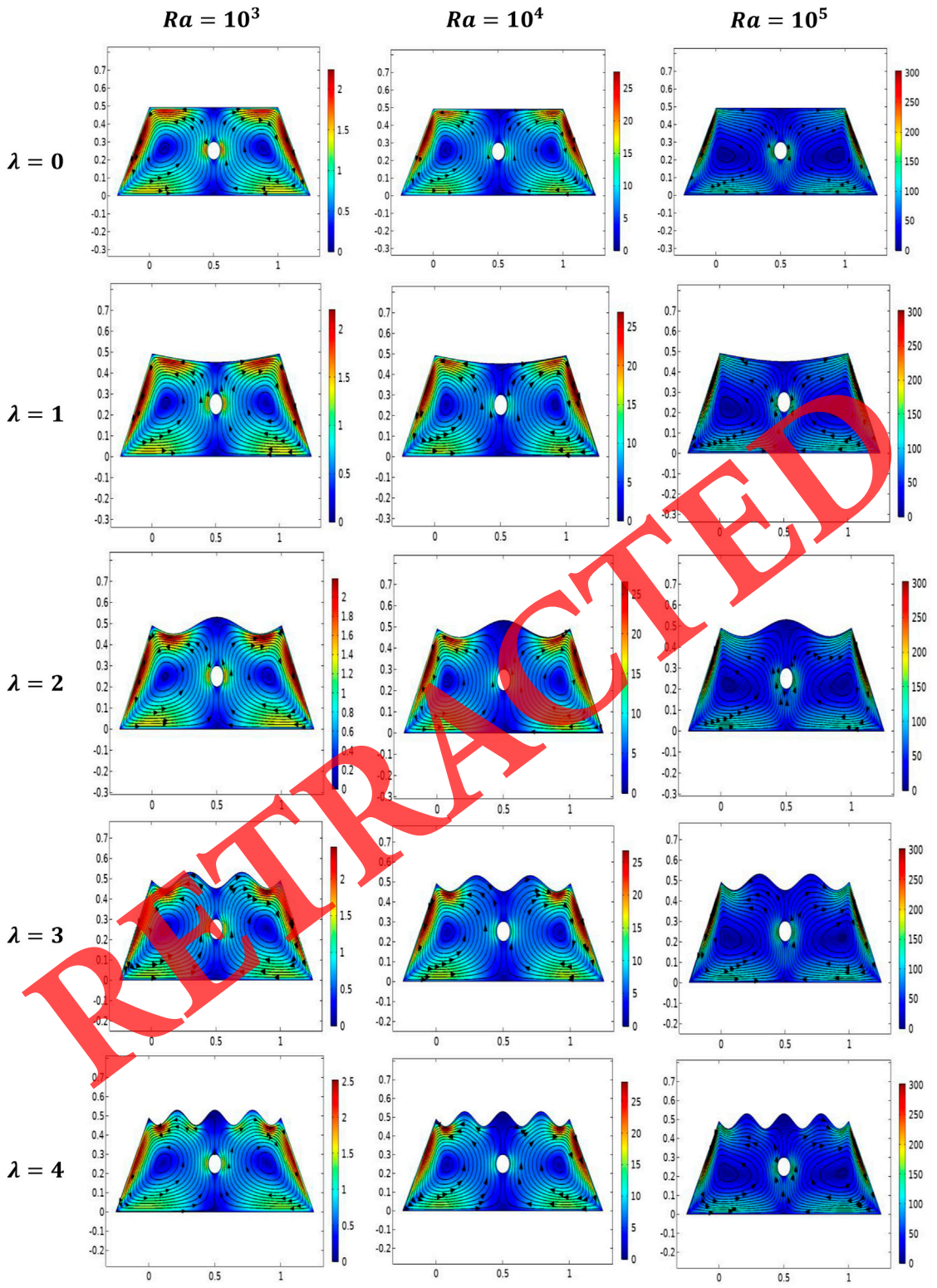

FIGURE 9
Streamline variation for the number of undulations against the Rayleigh number (*Ra*).

circulations and deformation of these contours, which boosts heat transfer. Moreover, *Ra* is the ratio of buoyancy to viscous, and buoyancy forces become dominant by increasing *Ra*, which increases the magnitude of temperature rapidly. At the highest magnitude of $Ra = 10^5$, it makes a thin layer on the lower heated wall and covers the horizontal top adiabatic wall with a thick layer.

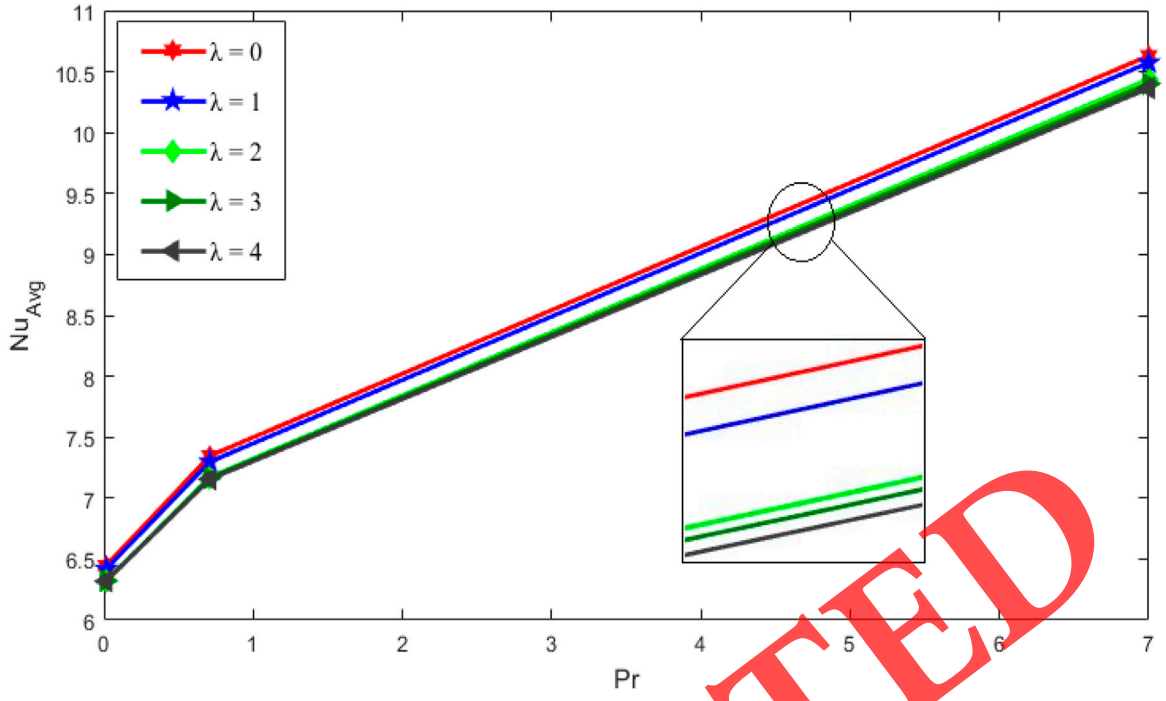

FIGURE 10
The influence of the Prandtl number (Pr) on the average Nusselt number (Nu_{Avg}) along the hot horizontal bottom wall and cylinder with various numbers of undulations (λ).

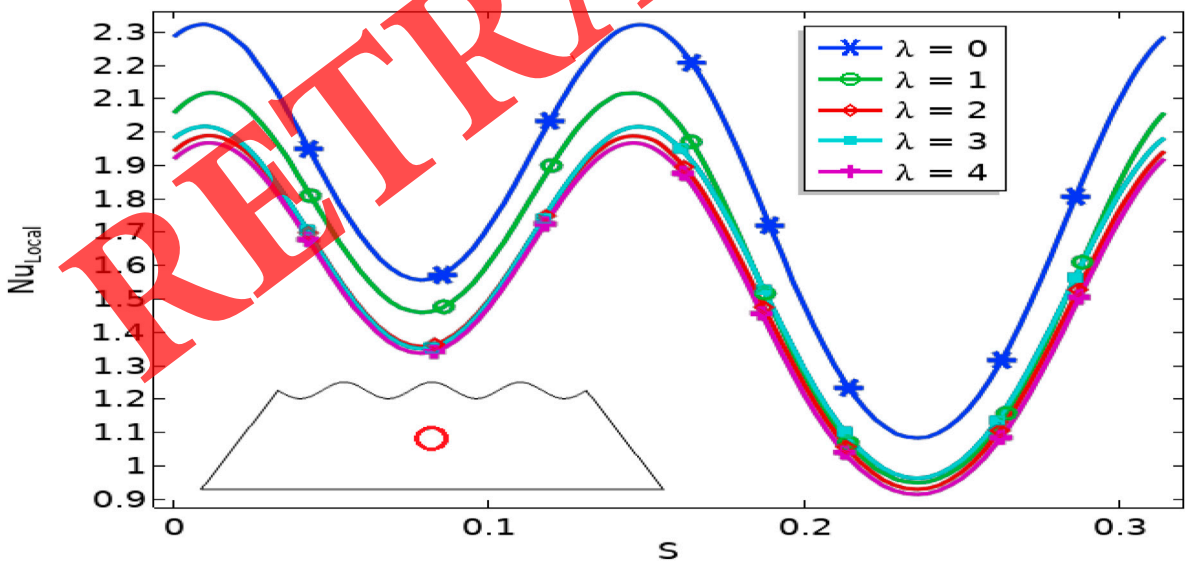

FIGURE 11
The influence of the number of undulations (λ) on local Nusselt number (Nu_{Local}) along the hot cylinder.

Furthermore, disclination in isothermal magnitude is depicted against the increasing number of undulations (λ). Again, it is established that at a lesser number of undulations $\lambda = 0$, temperature distribution enlarges on the top horizontal flat region, where at a higher value of $\lambda = 4$, the isothermal layers become thick at the base and thin on the horizontal top wavy region.

Figure 9 shows the coupled variation of the velocity field against the Rayleigh number (Ra) and number of undulations (λ), left to

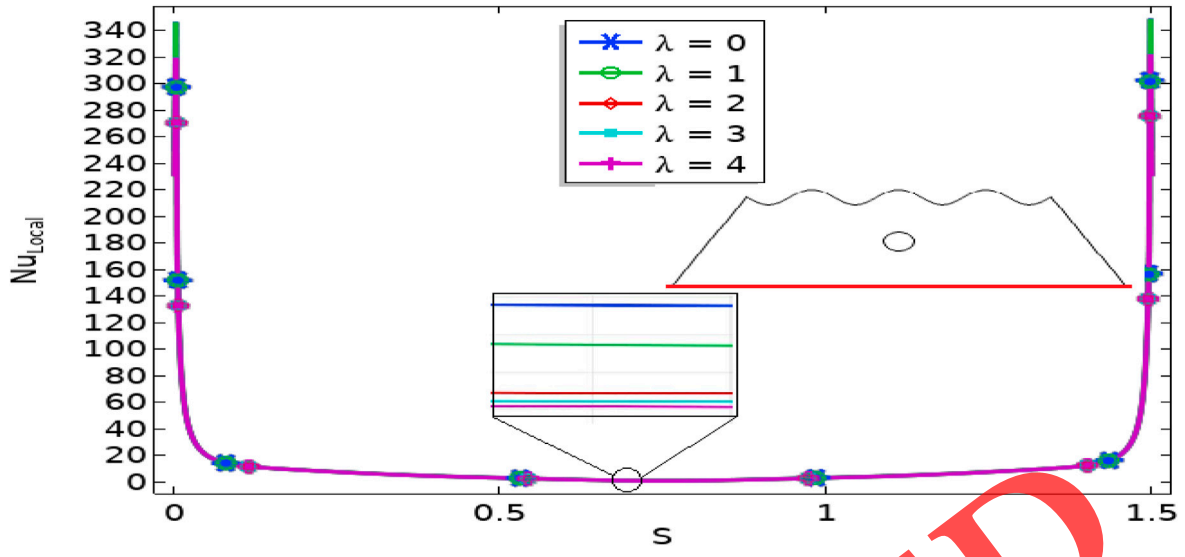

FIGURE 12
The influence of the number of undulations (λ) on the local Nusselt number (Nu_{Local}) along the horizontal heated bottom wall.

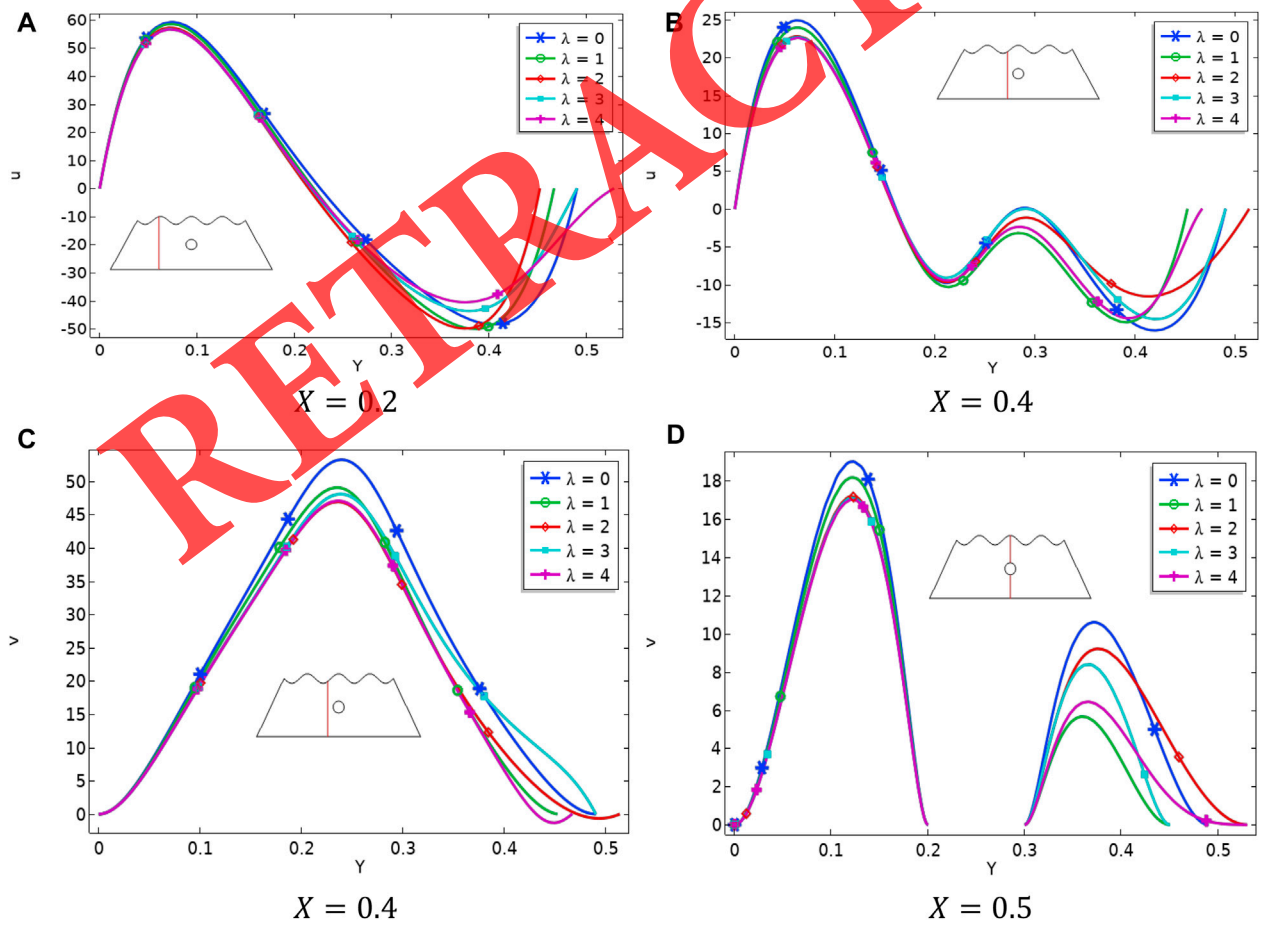

FIGURE 13
(A–D) Velocity variation against the number of undulations (λ) at various cutlines.

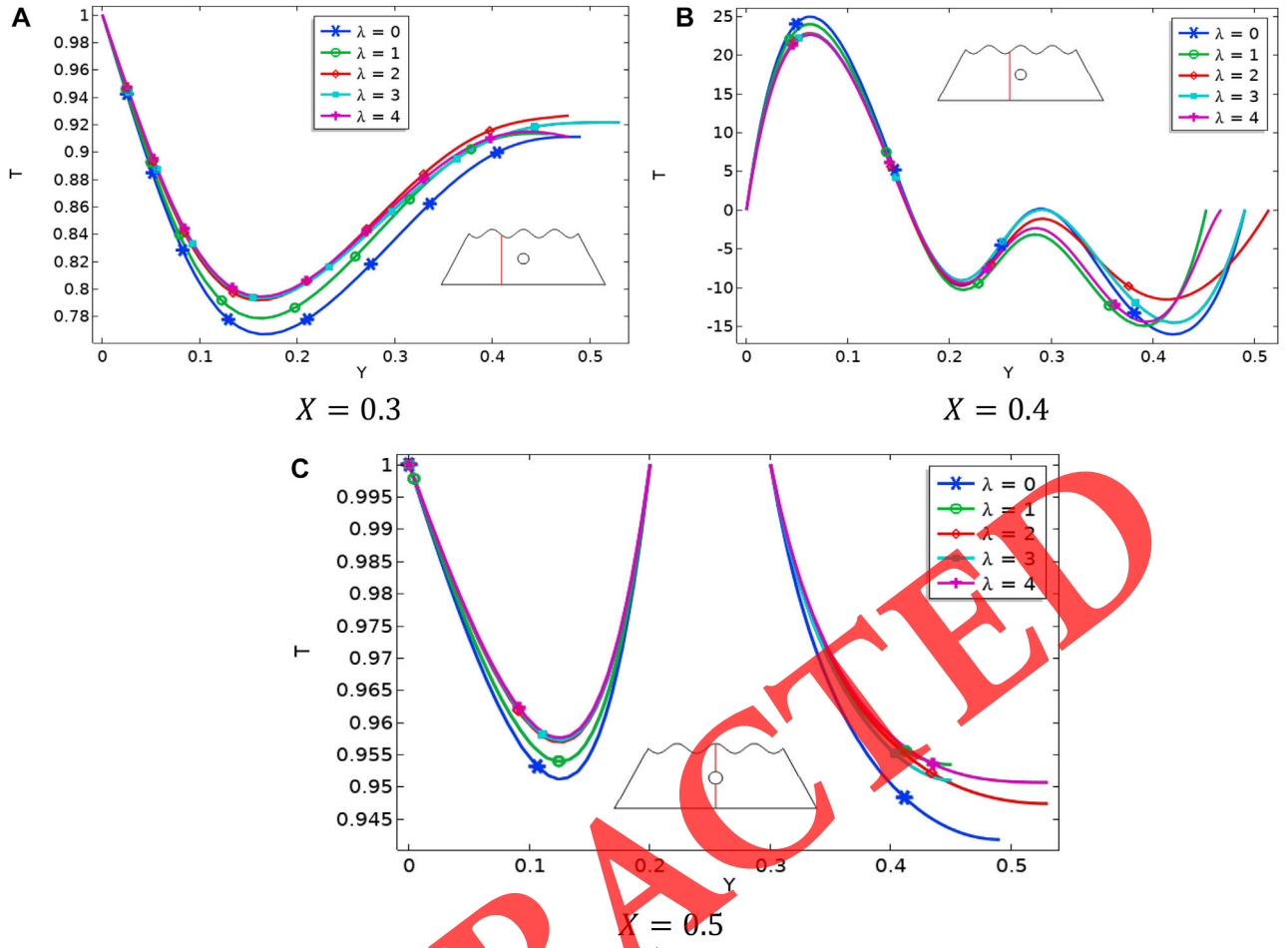

FIGURE 14
(A–C) Temperature variation against the number of undulations (λ) at various cutlines.

right and top to bottom, in view of the streamline field. It is observed that the streamlines raise from the horizontal heated wall with the heated cylinder and fall along the vertical cold wall forming two rolls within the left and right sides of the trapezoidal cavity rotating in anti-clockwise and clockwise directions. As Rayleigh number (Ra) has a direct relation with velocity, rolls become elliptic and cover up the whole cavity for the highest magnitude of Rayleigh number, i.e., ($Ra = 10^5$). Additionally, the increase in streamline magnitude is portrayed against the increasing number of undulations (λ) in the range of $0 \le \lambda \le 4$; five distinct numbers of undulations are entertained. However, the remaining parameters are kept constant by specifying the value of $Ra = 10^3$ and $P = 10^{-3}$. It is evident that the number of undulations has an inverse relationship with streamlines. By altering (λ) from 0 to 4, the top horizontal adiabatic wall will transition from a flat to a wavy surface. Two circular-shaped eddies are generated with the flat top of the adiabatic wall for $\lambda = 0$. The increase in λ from 1to 4 will change the flat surface into a wavy one, that is, crest and trough surface, and eddies enter the crest, decreasing the middle rotation's flow pattern and changing the shape of eddies from circular to elliptic.

Graphical visualization of variation in the average Nusselt number (Nu_{Avg}) against the Prandtl number (Pr) in the range of ($0.015 \le Pr \le 7.000$) and the number of undulations (λ) in the range of ($0 \le \lambda \le 4$) is depicted in Figure 11. For a lower magnitude of Pr, Pr less than 1, Nu_{avg} shows rapidly increasing aspects. However, Pr greater than 1 has slowly increasing change in Nu_{avg}, which shows increase in heat due to the convection mechanism. The number of undulations (λ) has an inverse relationship with the average Nusselt number (Nu_{avg}) because by increasing λ from 0 to 4, the average Nusselt Number (Nu_{Avg}) reduces.

Figure 11 shows the graphical description of the change in local heat flux coefficient against the number of undulations by considering the heated circular cylinder; here, the number of undulations varied from 0 to 4, representing the cases of non-undulations and undulations, respectively. It is expressively observed that by enhancing the number of undulations, the local Nusselt number (Nu_{Local}) depreciates because of the process of obstruction to the flow. These obstructions reduce the moment of a particle near the undulated surface, which causes velocity and associated kinetic energy and local heat flux. Therefore, it is concluded that maximum velocity is attended in the case of $\lambda = 0$, which represents the non-undulation case.

Figure 12 shows a visual explanation of the change in the local heat flux coefficient against the number of undulations by

TABLE 3 The influence of the Darcy number (P) on kinetic energy for various numbers of undulations (λ) at cutline ($X = 0.2$).

$K.E_{X=0.2}$					
P	$\lambda = 0$	$\lambda = 1$	$\lambda = 2$	$\lambda = 3$	$\lambda = 4$
$\mathbf{10^{-3}}$	364.810	362.710	338.740	315.110	303.820
$\mathbf{10^{-4}}$	19.7460	18.9430	17.4540	16.3980	15.3440
$\mathbf{10^{-5}}$	0.21646	0.20627	0.20219	0.19412	0.16906

Bold values means that the variation are measured against that parameters specially.

considering the horizontally heated bottom wall. Here, the number of undulations varied from 0 to 4, which represents the cases of non-undulations and undulations, respectively. The increase in the number of undulations leads the local Nusselt number (Nu_{Local}) to depreciate as a result of flow blockage. The local heat flux, kinetic energy, and moment of a particle near the undulating surface are reduced by these obstructions. Therefore, the case of $\lambda = 0$, which represents the non-undulation condition, has the maximum velocity.

Variation in kinetic energy in a comparative manner for non-undulated ($\lambda = 0$) and undulated ($\lambda \neq 0$) situations against the Darcy number (P) is elaborated in Table 3. It is enumerated that by decreasing the permeability parameter (P), kinetic energy decreases, whereas the opposite trend is observed against the number of undulations (λ). Decrementing aptitude of $K.E$ is observed due to recursion in pores of the medium in the decrementing Darcy number (P) due to which wavy face reduces as an outcome velocity, as well as associated $K.E$ down surge. Here, it is manifested that whenever $\lambda = 0$, the top horizontal surface of the enclosure becomes non-undulating and does not block the flow, the maximum value of K.E is reached.

The influence of horizontal and vertical components of velocity (u, v) at different positions in the enclosure against the number of undulations (λ) is depicted in Figures 13A–D. For measuring the optimum change in velocity, cut lines are drawn at $X = 0.2, X = 0.4$ for the horizontal component of velocity (u) and at $X = 0.4, X = 0.5$ for the vertical component of velocity (v) along with variation in Y from 0 to 0.55. Here, the number of undulations varies in the range of $0 \leq \lambda \leq 4$ and other parameters, such as $Pr = 0.710$, $P = 10^{-3}$, and $Ra = 10^3$, are kept constant. It is observed from the sketches that by increasing λ from 0 to 4, velocity decreases.

The influence of temperature distribution (T) at different positions in the enclosure against the number of undulations (λ) is manifested in Figures 14A–C. Fluctuating behavior of temperature distribution is seen at different positions in the enclosure.

5 Concluding remarks

In the current discussion, the attributes of the Newtonian fluid flow in a permeable trapezoidal domain using a uniformly heated horizontal bottom wall and circular cylinder at the center of the enclosure and top horizontal adiabatic wavy wall are stated. The mathematical formulation of the problem involved is acknowledged in the context of intricate dimensionless partial differential structure. Subsequently, these differential equations are determined by applying the Galerkin finite element procedure. The Tabular analysis of degrees of freedom and the number of elements containing discretization of the domain is accumulated.

The crucial findings are as follows:

1. Upsurge in kinetic energy is revealed against the increment in Darcy number.
2. Depreciation in kinetic energy and heat flux coefficient is found against escalation in the number of undulations.
3. Circulations in flow phenomenon raise against uplift in Rayleigh and Darcy numbers due to the production of thermal buoyancy forces and reduction in viscous forces, respectively.
4. Heat flux coefficient is the least in the presence of undulation, whereas contrary behavior is found when undulations on the surface are removed.
5. It is depicted that the velocity field adheres to the low magnitude when it interacts with the trough of the undulated wall in comparison to its interaction with the crest of the surface.
6. It is observed that the installation of a heated circular cylinder plays an essential role in transmission of heat in the domain.

Data availability statement

The raw data supporting the conclusion of this article will be made available by the authors without undue reservation.

Author contributions

SB: conceptualization, result acquisition, and code validation; NK: result acquisition, formal analysis, and writing; SE; analysis, post-processing of results, and fund acquisition.

Conflict of interest

The authors declare that the research was conducted in the absence of any commercial or financial relationships that could be construed as a potential conflict of interest.

Publisher's note

All claims expressed in this article are solely those of the authors and do not necessarily represent those of their affiliated organizations or those of the publisher, the editors, and the reviewers. Any product that may be evaluated in this article, or claim that may be made by its manufacturer, is not guaranteed or endorsed by the publisher.

References

1. Beavers GS, Joseph DD. Boundary conditions at a naturally permeable wall. *J Fluid Mech* (1967) 30:197–207. doi:10.1017/s0022112067001375

2. Poulikakos D, Bejan A, Selimos B, Blake KR. High Rayleigh number convection in a fluid overlaying a porous bed. *Int J Heat Fluid Flow* (1986) 7:109–16. doi:10.1016/0142-727x(86)90056-1

3. Beckermann C, Ramadhyani S, Viskanta R. Natural convection flow and heat transfer between a fluid layer and a porous layer inside a rectangular enclosure. *J Heat Transfer* (1987) 109:363–70.

4. Beckermann CH, Viskanta R, Ramadhyani S. Natural convection in vertical enclosures containing simultaneously fluid and porous layers. *J Fluid Mech* (1988) 186:257–84. doi:10.1017/s0022112088000138

5. Chen F, Chen CF. Experimental investigation of convective stability in a superposed fluid and porous layer when heated from below. *J Fluid Mech* (1989) 207:311–21. doi:10.1017/s0022112089002594

6. Breton PL, Caltagirone JP, Arquis E. Natural convection in a square cavity with thin porous layers on its vertical walls. *J Heat Transfer* (1991) 113:892–8.

7. Singh AK, Thorpe GR. Natural convection in a confined fluid overlying a porous layer-a comparison. *Indian J Pure Appl Math* (1995) 26:81–95.

8. Webster IT, Norquay SJ, Ross FC, Wooding RA. Solute exchange by convection within estuarine sediments. *Estuarine, Coastal Shelf Sci* (1996) 42:171–83. doi:10.1006/ecss.1996.0013

9. Goyeau B, Lhuillier D, Gobin D, Velarde MG. Momentum transport at a fluid–porous interface. *Int J Heat Mass Transfer* (2003) 46:4071–81. doi:10.1016/s0017-9310(03)00241-2

10. Gobin D, Goyeau B, Neculae A. Convective heat and solute transfer in partially porous cavities. *Int J Heat Mass Transfer* (2005) 48:1898–908. doi:10.1016/j.ijheatmasstransfer.2004.12.016

11. Shah Z, Ullah A. Ferrofluid treatment with insertion of electric field inside a porous cavity considering forced convection. *Waves in Random and Complex Media* (2023) 2023:1–19. doi:10.1080/17455030.2023.2169386

12. Lund LA, Chandio AF, Vrinceanu N, Yashkun U, Shah Z, Alshehri A. Darcy–Forchheimer magnetized nanofluid flow along with heating and dissipation effects over a shrinking exponential sheet with stability analysis. *Micromachines* (2022) 14:106. doi:10.3390/mi14010106

13. Rooman M, Jameel M, Tassaddiq A, Shah Z, Alshehri A, Kumam P. Significance of variable viscosity and thermal conductivity on the dynamics of MHD cross nanofluid over a stratified Darcy-Forchheimer porous surface of a paraboloid of revolution subjected to entropy generation. *Int Commun Heat Mass Transfer* (2022) 139(2022):106464. doi:10.1016/j.icheatmasstransfer.2022.106464

14. Chamkha AJ, Khaled ARA. Hydromagnetic combined heat and mass transfer by natural convection from a permeable surface embedded in a fluid-saturated porous medium. *Int J Numer Methods Heat Fluid Flow* (2000) 10(5):455–77. doi:10.1108/09615530010338097

15. Goering DJ, Kumar P. Permeability effects on winter-time natural convection in gravel embankments. In: *Advances in cold-region thermal engineering and sciences*. Berlin, Heidelberg: Springer (1999). p. 455–64.

16. Zhang Z, Bejan A, Lage JL. Natural convection in a vertical enclosure with internal permeable screen. *J Heat Transfer* (1991) 113:377–83.

17. Ngo CC, Lai FC. Effective permeability for natural convection in a layered porous annulus. *J Thermophys Heat transfer* (2000) 14(3):363–7. doi:10.2514/2.6533

18. Yih KA. Coupled heat and mass transfer by natural convection adjacent to a permeable horizontal cylinder in a saturated porous medium. *Int Commun Heat mass transfer* (1999) 26(3):431–40. doi:10.1016/s0735-1933(99)00029-9

19. Kiwan S, Zeitoun O. Natural convection in a horizontal cylindrical annulus using porous fins. *Int J Numer Methods Heat Fluid Flow* (2008) 18:618. doi:10.1108/09615530810879747

20. Fand RM, Steinberger TE, Cheng P. Natural convection heat transfer from a horizontal cylinder embedded in a porous medium. *Int J Heat Mass Transfer* (1986) 29(1):119–33. doi:10.1016/0017-9310(86)90040-2

21. Nield DA, Adrian B. *Convection in porous media*. New York: Springer (2006).

22. Ratouis TMP, Zarrouk SJ. Factors controlling large-scale hydrodynamic convection in the Taupo Volcanic Zone (TVZ), New Zealand. *Geothermics* (2016) 59:236–51. doi:10.1016/j.geothermics.2015.09.003

23. Cheng P. Heat transfer in geothermal systems. *Adv Heat transfer* (1979) 14:1–105. doi:10.1016/S0065-2717(08)70085-6

24. Molla MM, Saha S, Khan MAI. Natural convection flow in a porous enclosure with localized heating from below. *JP J Heat Mass Transfer* (2012) 6:1–16.

25. Alhashash A, Saleh H. Natural convection induced by undulated surfaces in a porous enclosure filled with nanoliquid. *Adv Mech Eng* (2019) 9:168781401987528. doi:10.1177/1687814019875284, no.

26. Dawar A, Islam S, Shah Z, Alshehri A, Mahmuod SR. A numerical study of the micropolar nanofluid flow containing aluminum alloy nanoparticles over a variable thickened stretching sheet. *Int J Mod Phys B* (2022) 2022:2350197. doi:10.1142/s0217979223501977

27. Hussain S, Rasheed K, Ali A, Vrinceanu N, Alshehri A, Shah Z. A sensitivity analysis of MHD nanofluid flow across an exponentially stretched surface with non-uniform heat flux by response surface methodology. *Scientific Rep* (2022) 12:18523. doi:10.1038/s41598-022-22970-y

28. Bejan A. On the boundary layer regime in a vertical enclosure filled with a porous medium. *Lett Heat Mass Transfer* (1979) 6:93–102. doi:10.1016/0094-4548(79)90001-8

29. Prasad V, Kulacki FA. Convective heat transfer in a rectangular porous cavity—Effect of aspect ratio on flow structure and heat transfer. *J Heat Transfer* (1984) 106:158–65.

30. Lai FC, Kulacki FA. Natural convection across a vertical layered porous cavity. *Int J Heat mass transfer* (1988) 31:1247–60. doi:10.1016/0017-9310(88)90067-1

31. Bilal SM, Khan NZ, Riaz A, Alyami MA, Din EME. Measure and evaluate the hydrothermal flow of a Newtonian fluid in homogeneous permeable media equipped with a fin: A numerical approach. *Front Phys* (2022) 10(2022):1129. doi:10.3389/fphy.2022.1032437